The present work is carried out at the University of Latvia and has been supported by the European Regional Development Fund project № 2013/0051/2DP/2.1.1.1.0/13/APIA/VIAA/009

EIROPAS REĢIONĀLĀS ATTĪSTĪBAS FONDS

EIROPAS SAVIENĪBA

IEGULDĪJUMS TAVĀ NĀKOTNĒ

Modelling of pattern formation during the melting of silicon by HF EM field

Kristaps Bergfelds, Jānis Virbulis, Armands Krauze

9th PAMIR International Conference of Fundamental and Applied MHD
University of Latvia, Raina Blvd. 19, Riga, Latvia
17.06.2014.

Contents

- Problem description – inhomogeneous melting during floating zone crystal growth.
- Method of research – description of mathematical model and its implementation.
- Results – numerical calculations using the developed program.
- Conclusions – interpretation of calculation results.

Problem description

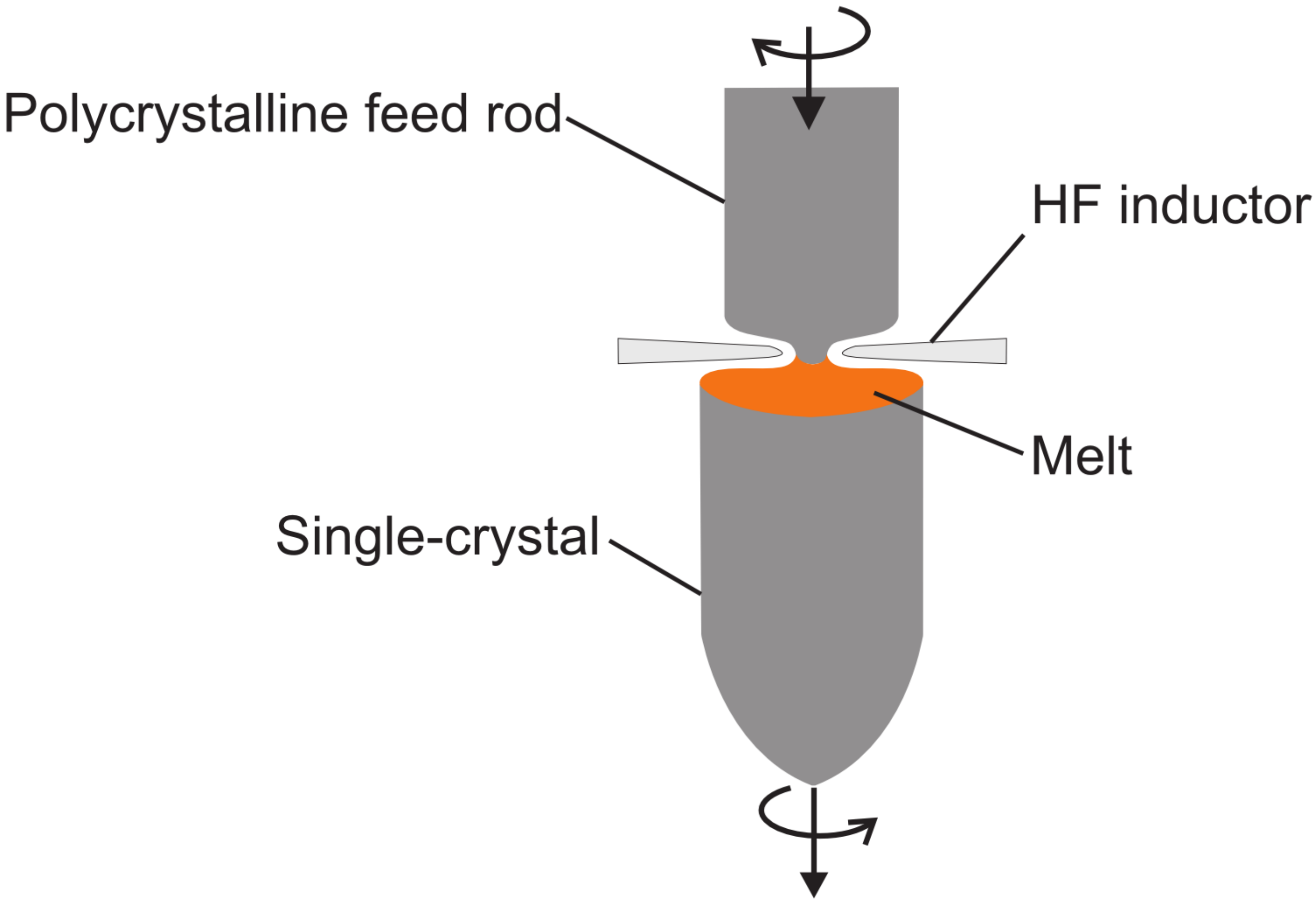

Fig. 1: Schematics of floating zone (FZ) crystal growth process.

Problem description

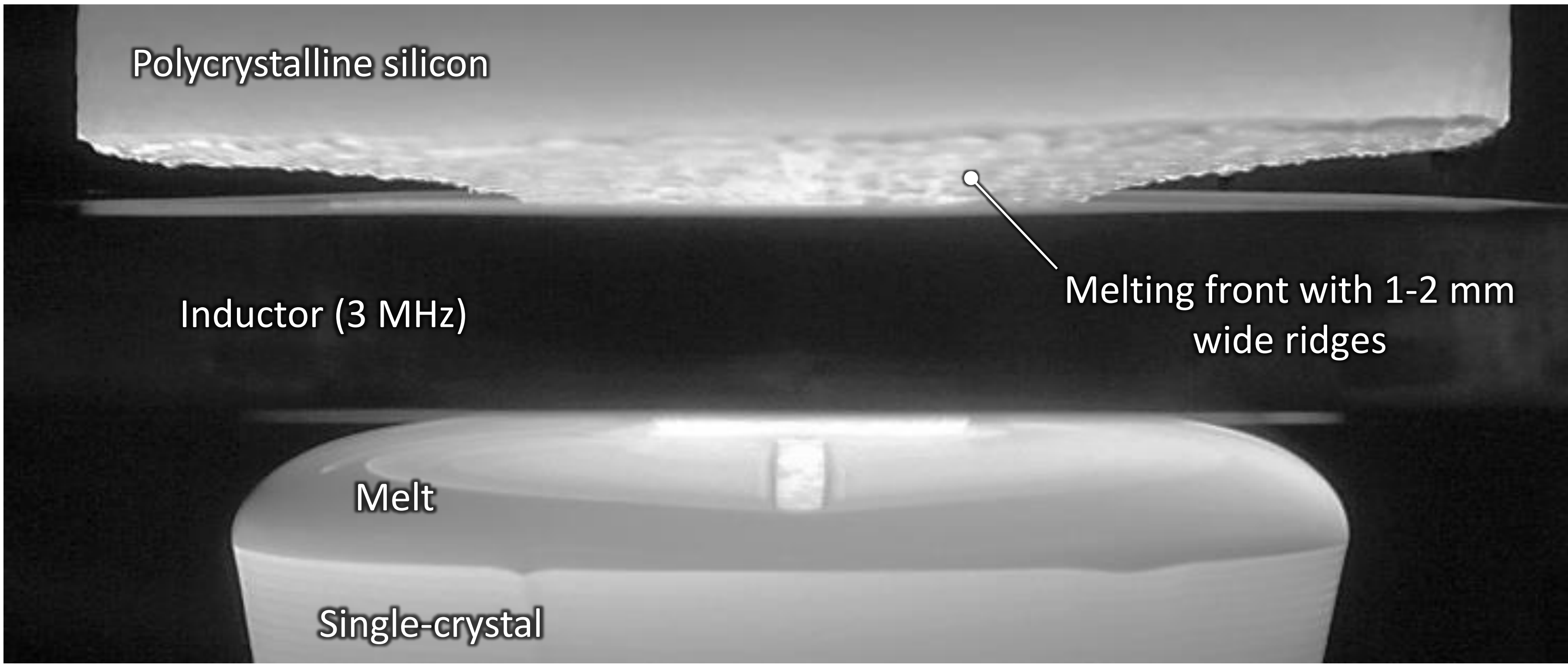

Fig. 2: Photography of the floating-zone process where inhomogeneous melting process can be observed[1].

1 – **Thierry Duffar**, editor. *Crystal Growth Processes Based on Capillarity: Czochralski, Floating Zone, Shaping and Crucible Techniques.* Wiley-Blackwell, 2010.

Problem description

- To ensure stable FZ process, it is necessary to understand the non-uniform melting.
- Some authors[2] suggest that melt flow is a determining factor for the shape of the melting front.
- However, present work suggests that melt patterns is created due to induced current localization within melt regions.
- Underlying cause is the electrical conductivity σ and skin-depth δ differences for silicon melt and solid.
  - solid: $\sigma = 5.0 \cdot 10^4\ \mathrm{S/m}$ $\delta = 1.30\ \mathrm{mm}$
  - melt: $\sigma = 1.2 \cdot 10^6\ \mathrm{S/m}$ $\delta = 0.27\ \mathrm{mm}$

2 – **Thierry Duffar**, editor. *Crystal Growth Processes Based on Capillarity: Czochralski, Floating Zone, Shaping and Crucible Techniques.* Wiley-Blackwell, 2010.

Mathematical model

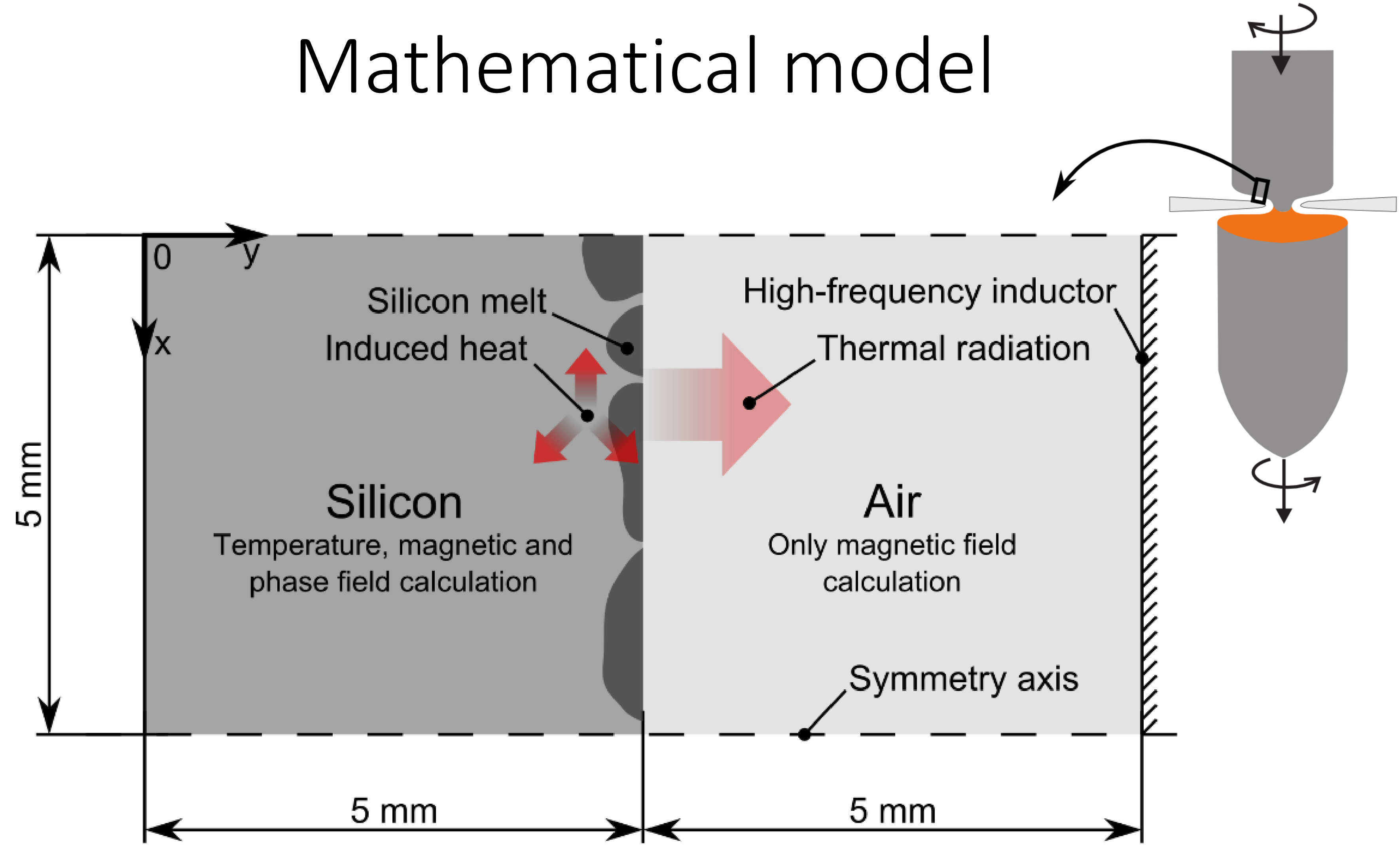

Fig. 3: Schematics of the modelled region and physical processes in it.

Mathematical model

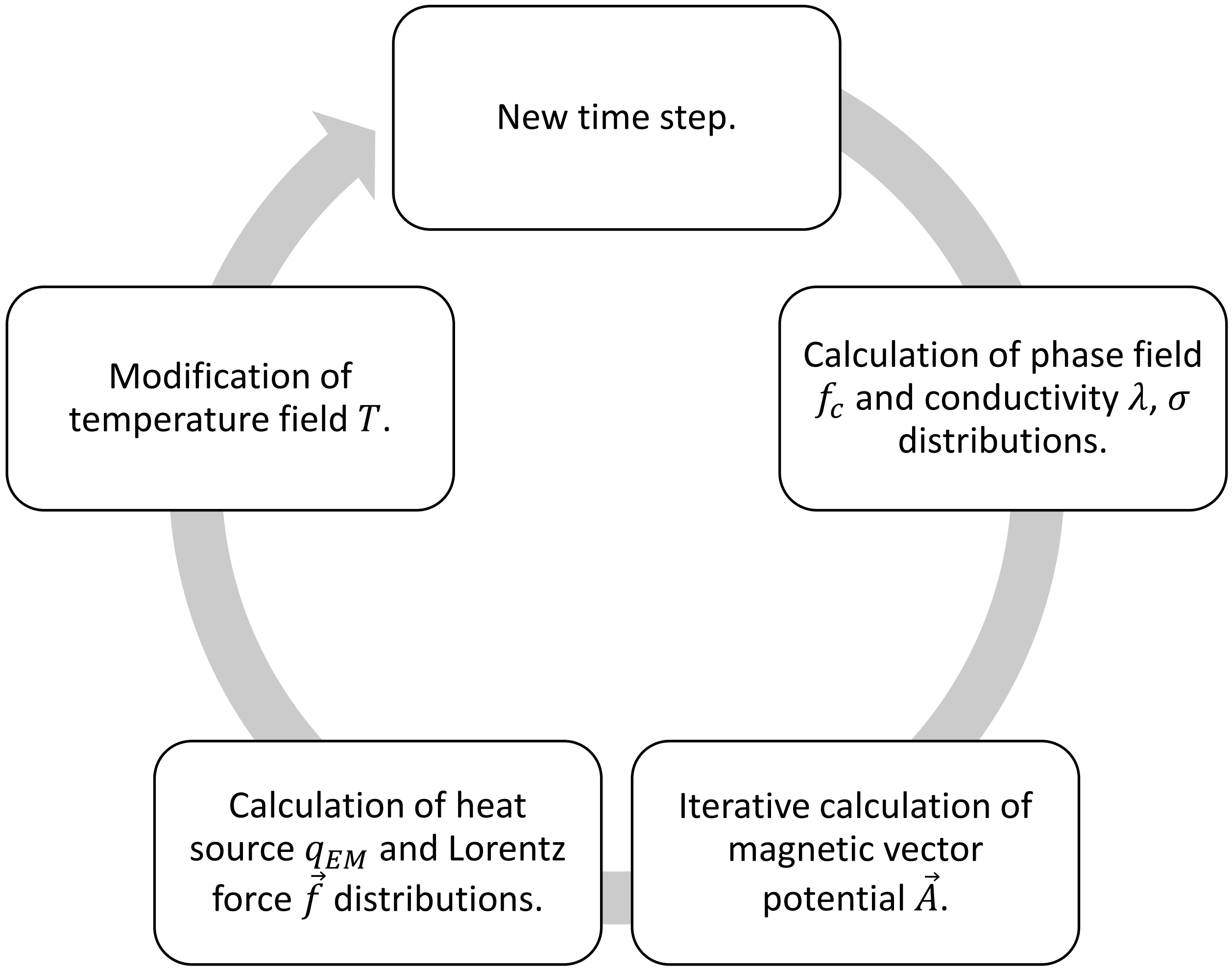

Fig. 4: Algorithm for the non-stationary calculation software implemented with *Matlab/Octave* language.

Mathematical model

- Phase field calculation[3]

$$f_c = \begin{cases} 0 & \text{if} \quad T > T_0 + \frac{\Delta T_s}{2} \\ \frac{T_0 + \frac{\Delta T_s}{2} - T}{\Delta T_s} & \text{if} \quad T \geq T_0 - \frac{\Delta T_s}{2} \text{ and } T \leq T_0 + \frac{\Delta T_s}{2} \\ 1 & \text{if} \quad T < T_0 - \frac{\Delta T_s}{2} \end{cases}$$

- Temperature field calculation

$$\left(\rho c_p - L \frac{\mathrm{d} f_c}{\mathrm{d}T}\right) \frac{\partial T}{\partial t} = \lambda \Delta T + q_{\mathrm{EM}}$$

$$\frac{\varepsilon \sigma_{\mathrm{SB}} T^4}{\lambda} = \frac{\partial T}{\partial y}\bigg|_{y=5\,\mathrm{mm}} \qquad 0 = \frac{\partial T}{\partial x}\bigg|_{x=0\,\mathrm{mm}} \qquad 0 = \frac{\partial T}{\partial x}\bigg|_{x=5\,\mathrm{mm}}$$

3 – **I. Steinbach et al.** Numerical simulations for silicon crystallization processes — examples from ingot and ribbon casting. *Solar Energy Materials and Solar Cells*, 72(1–4):59–68, 2002.

Mathematical model

- Magnetic vector potential

$$\Delta\vec{A} - i\omega\sigma\mu\vec{A} = \vec{0} \qquad 0 = A_z\Big|_{y=0\,\mathrm{mm}} \quad k_I = A_z\Big|_{y=10\,\mathrm{mm}}$$

- Current density, heat sources, magnetic field

$$j_z = -i\sigma\omega A_z \qquad q_{\mathrm{EM}} = \frac{|j_z|^2}{2\sigma} \qquad \vec{B} = (B_x, B_y, B_z) = \left(\frac{\partial A_z}{\partial y}, -\frac{\partial A_z}{\partial x}, 0\right)$$

- Time-averaged Lorentz force density

$$\overline{f_x} = -\frac{1}{2}\Re(j_z)\Re(B_y) - \frac{1}{2}\Im(j_z)\Im(B_y)$$

$$\overline{f_y} = +\frac{1}{2}\Re(j_z)\Re(B_x) + \frac{1}{2}\Im(j_z)\Im(B_x)$$

Results demonstrating localization of induced heat sources

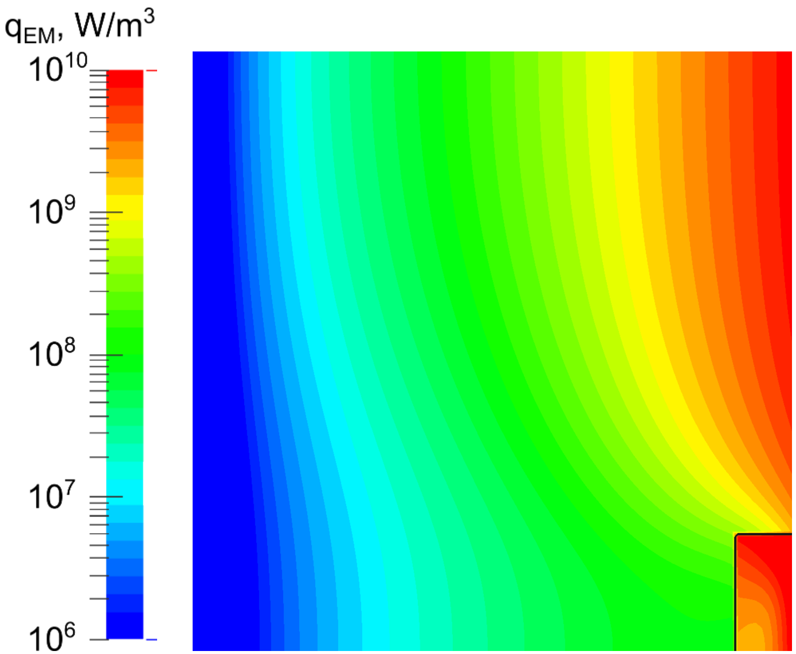

Fig. 5: Induced heat source density distribution influenced by melt presence within the system.

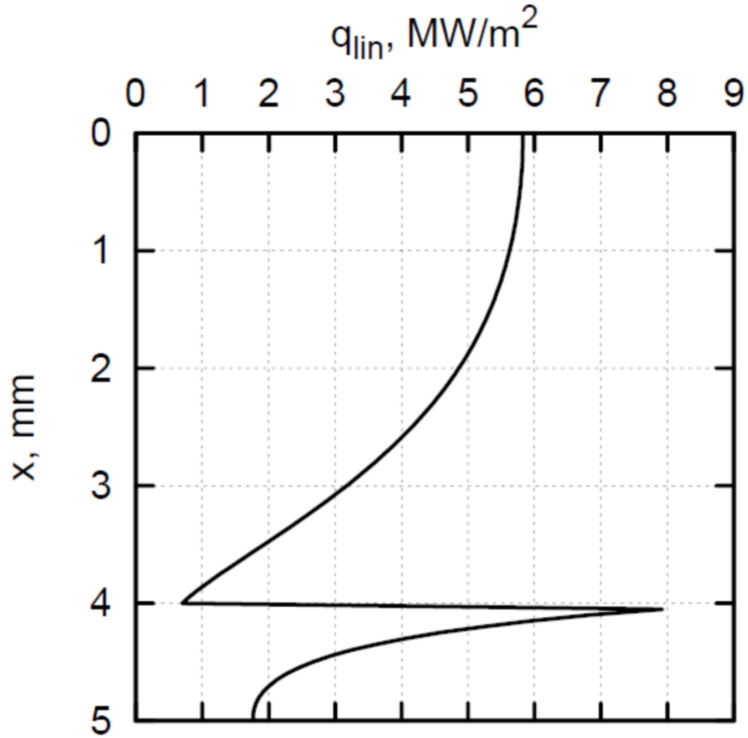

Fig. 6: Surface heat source density along the vertical axis in Fig. 5.

Transient calculation results with initial temperature field perturbation

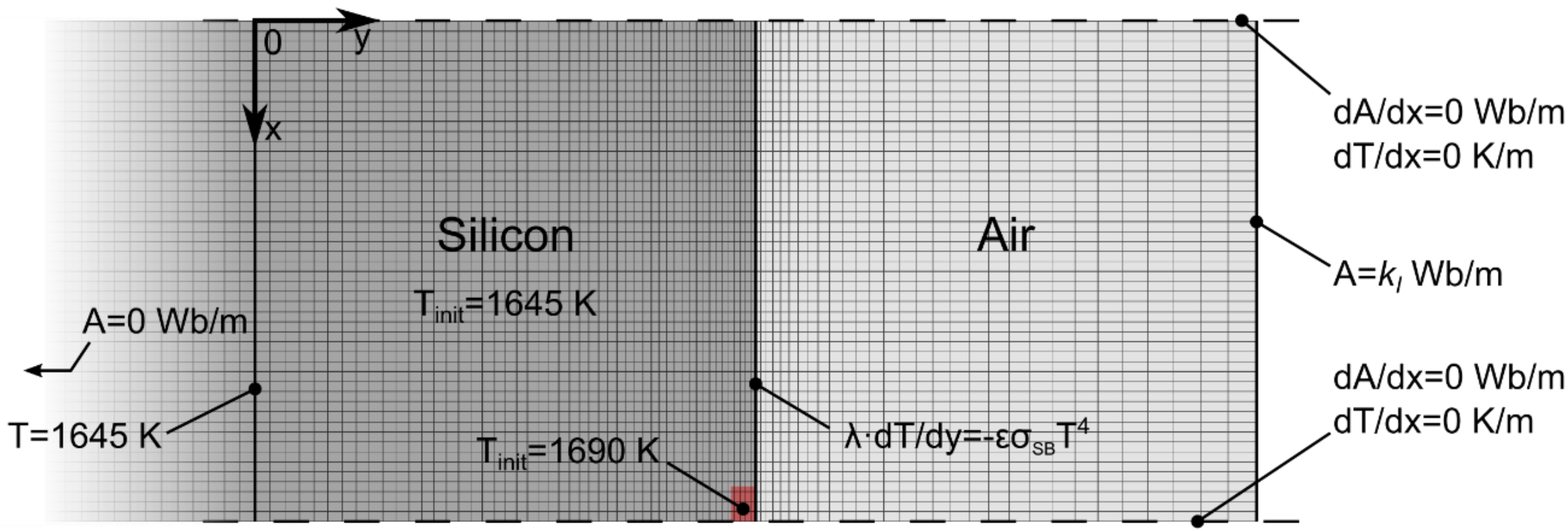

Fig. 7: Initial and boundary conditions for calculations with temperature field perturbation. Calculation mesh is also shown.

Transient calculation results with initial temperature field perturbation

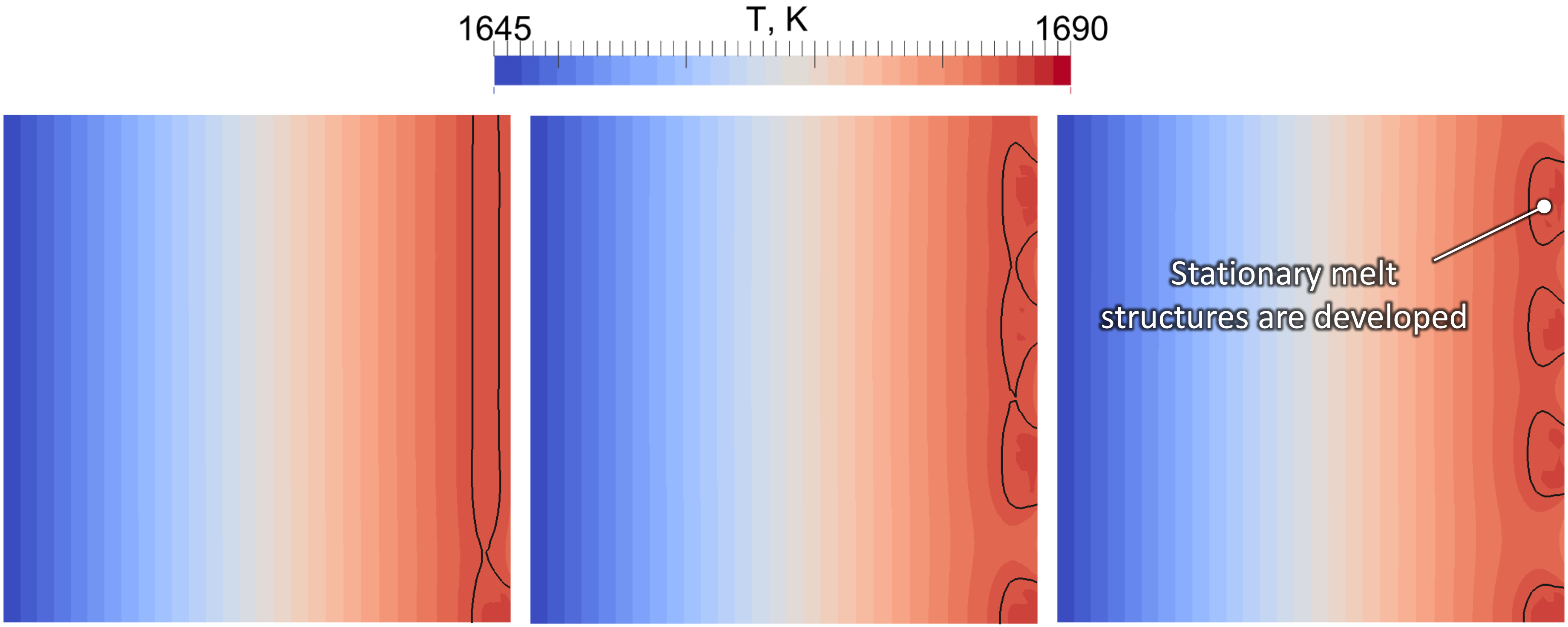

a) 5 s **b)** 15 s **c)** 20 s

Fig. 8: Different time instances of calculated temperature fields. Formation of melt structures is demonstrated. Black line represents phase boundary between silicon melt and solid.

Physical parameter influence on melt structure distance

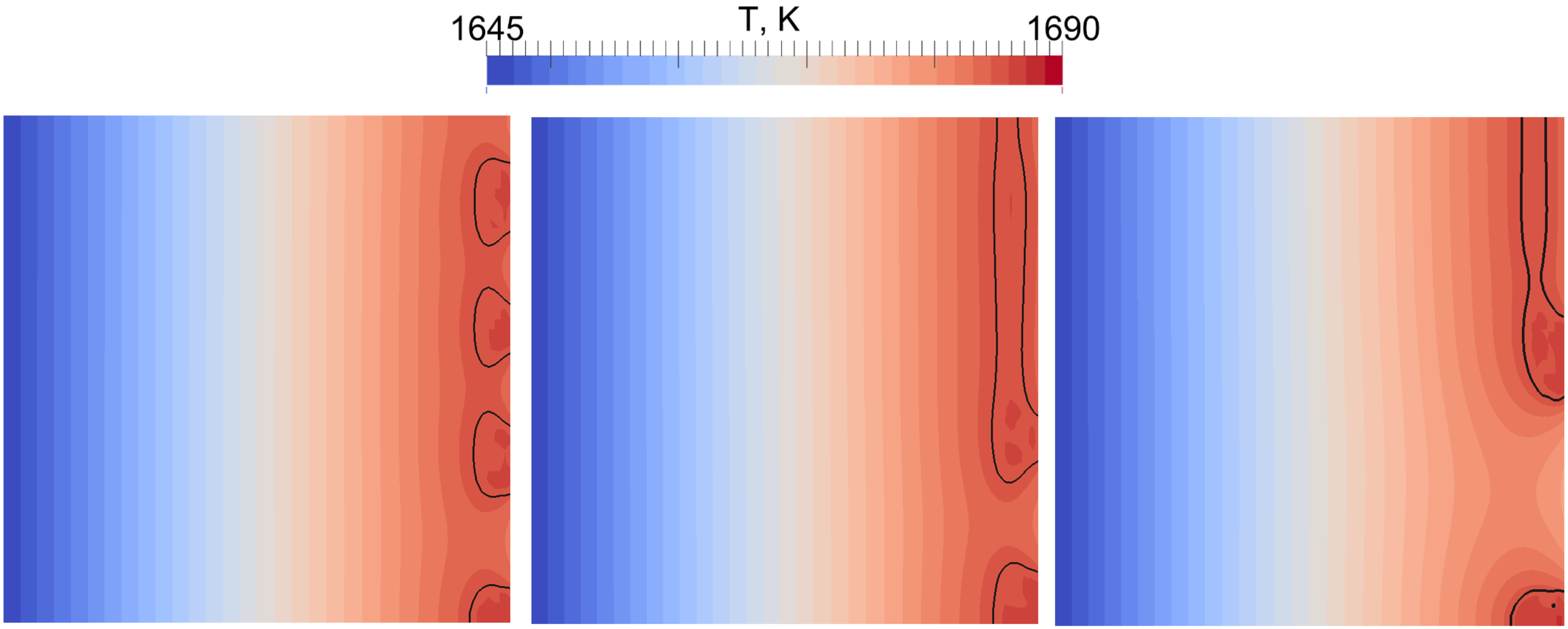

a) $\sigma_S = 5 \cdot 10^4$ S/m, $f = 3$ MHz **b)** $\sigma_S = 5 \cdot 10^4$ S/m, $f = 2$ MHz **c)** $\sigma_S = 1 \cdot 10^4$ S/m, $f = 3$ MHz

Fig. 9: Calculation results obtained by using different solid silicon electrical conductivities σ_S and magnetic field frequencies f.

Physical parameter influence on melt structure distance

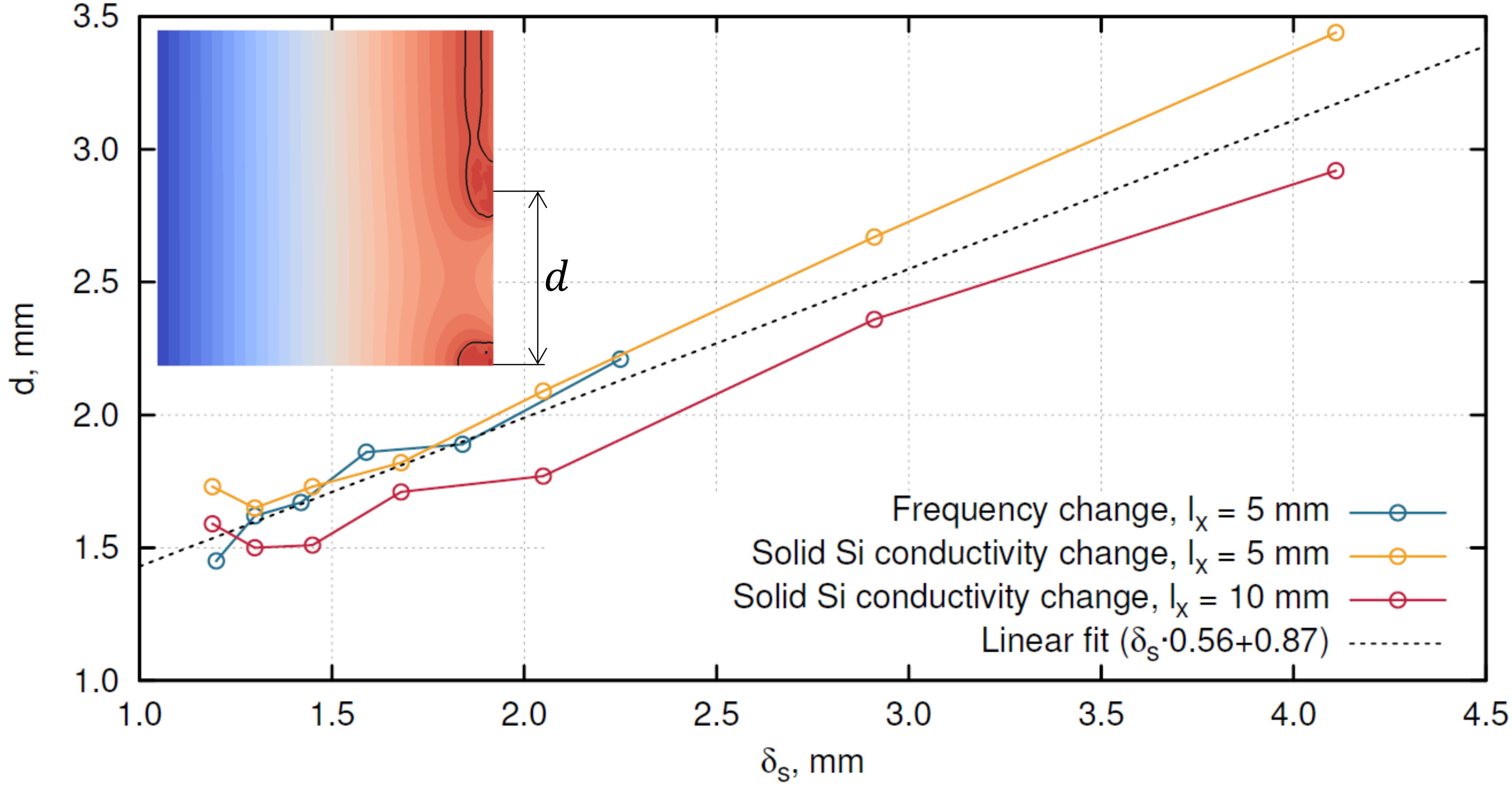

Fig. 10: Distance between melt structures d as a function of skin-depth in solid silicon δ_s.

Transient calculations with two-sided radiation

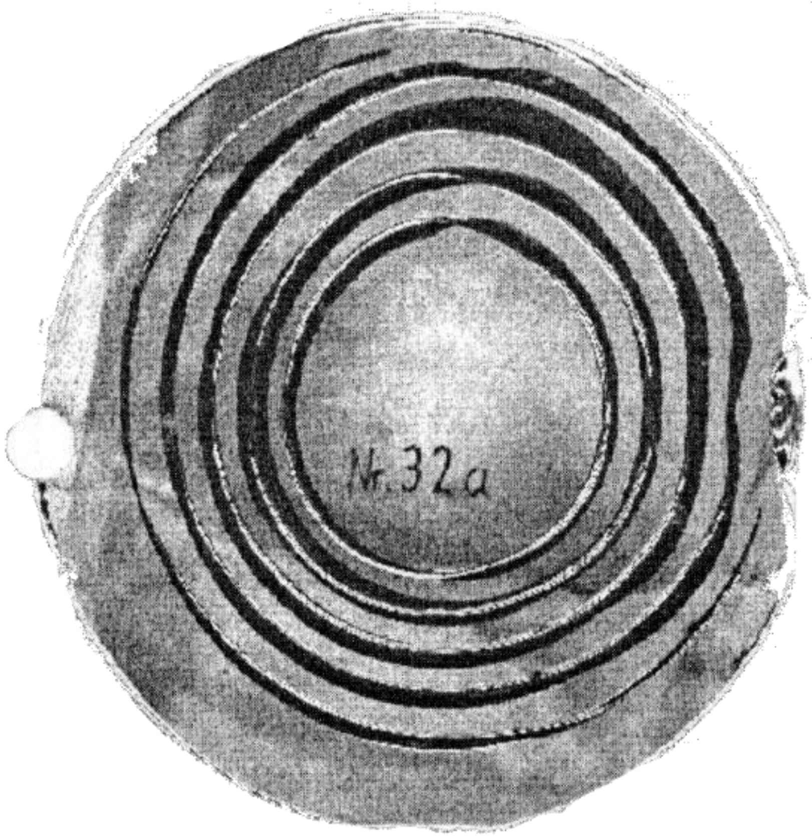

Fig. 11: Gredzenveida struktūras uz silīcija plāksnes, kas novietota zem AF induktora[4].

4 – **Helge Riemann et al.** Silicon floating zone process: Numerical modeling of RF field, heat transfer, thermal stress, and experimental proof for 4 inch crystals. *Journal of The Electrochemical Society*, 142(3):1007–1014, 1995.

Transient calculations with two-sided radiation

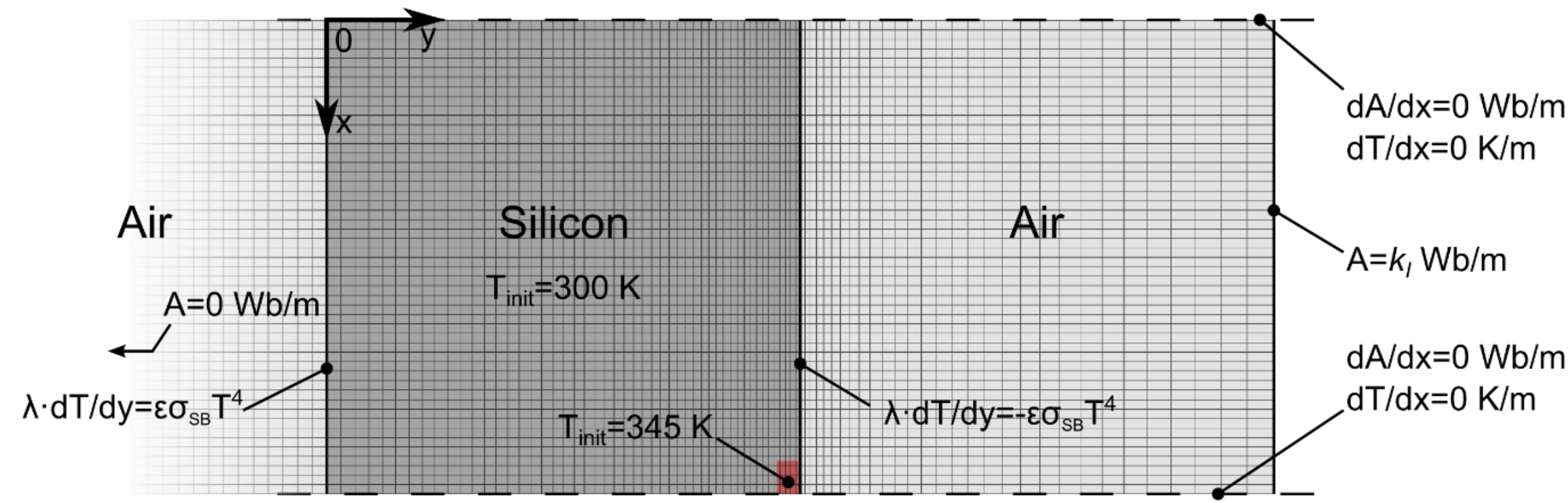

Fig. 12: Initial and boundary conditions for calculations with two-sided radiation. Calculation mesh is also shown.

Transient calculations with two-sided radiation

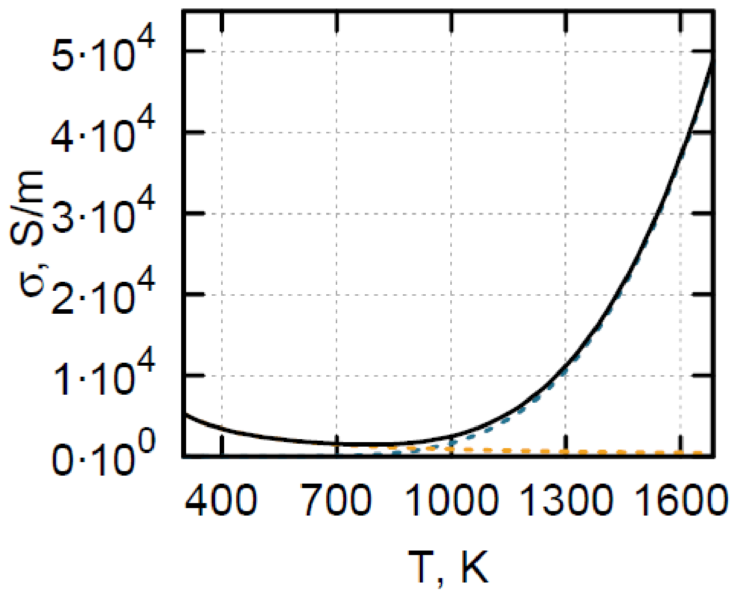

a) Linear scale

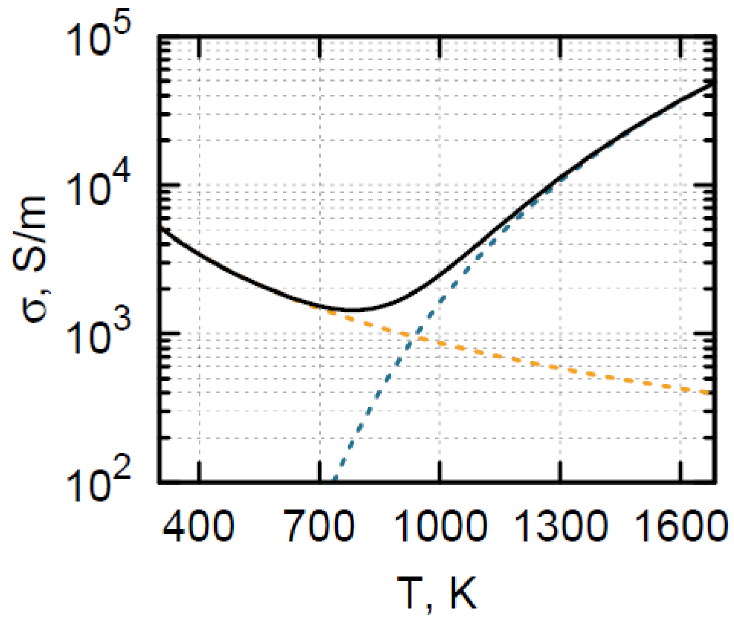

b) Logarithmic scale

Fig. 13: Plot of solid silicon electrical conductivity dependence on temperature (from $300\,\mathrm{K}$ to melt point of $1685\,\mathrm{K}$). Blue line – generation of conduction electrons, yellow – electron vacancy conductivity. Black line is the sum of both functions[5].

5 – **C. Kittel**. *Introduction to Solid State Physics*. Wiley, 8th edition, 2005.

Transient calculations with two-sided radiation

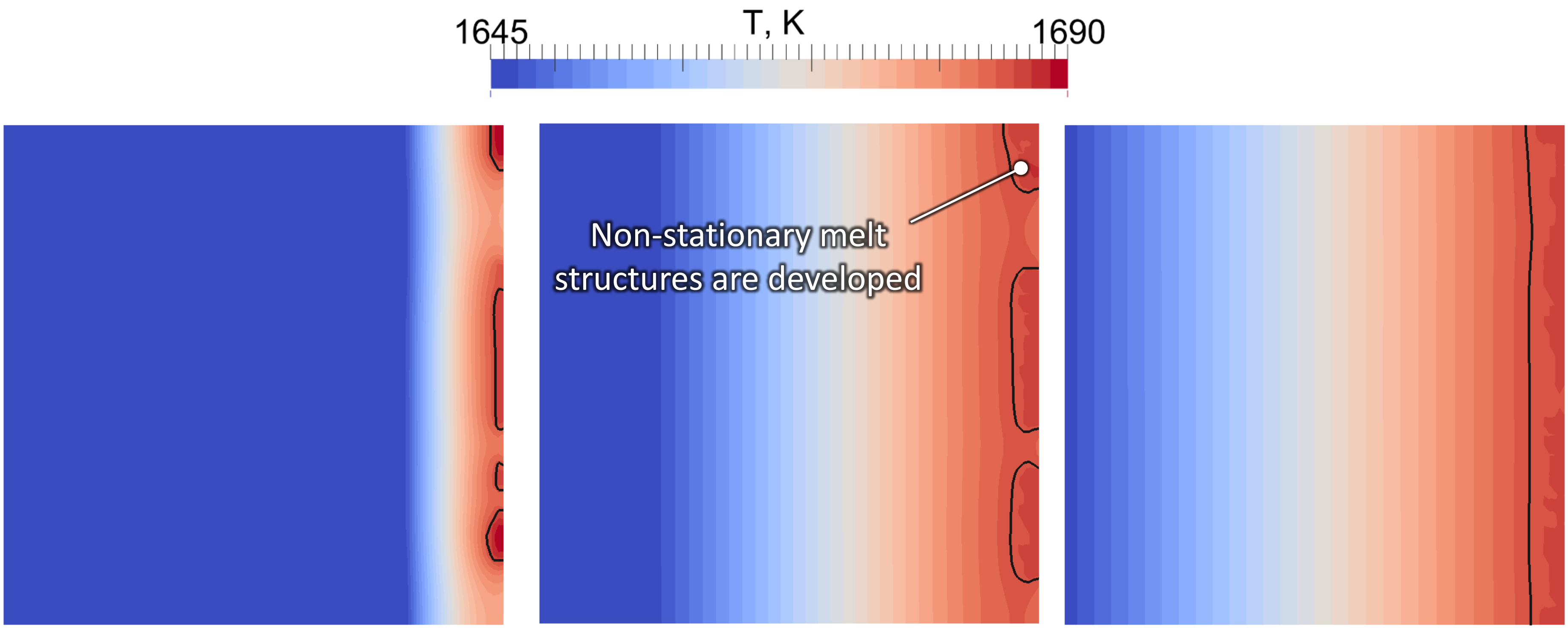

a) 2 s **b)** 4 s **c)** 10 s

Fig. 14: Different time instances of calculated temperature fields. Formation of melt structures is demonstrated. Black line represents phase boundary between silicon melt and solid.

Analysis of melt structure interaction with EM field

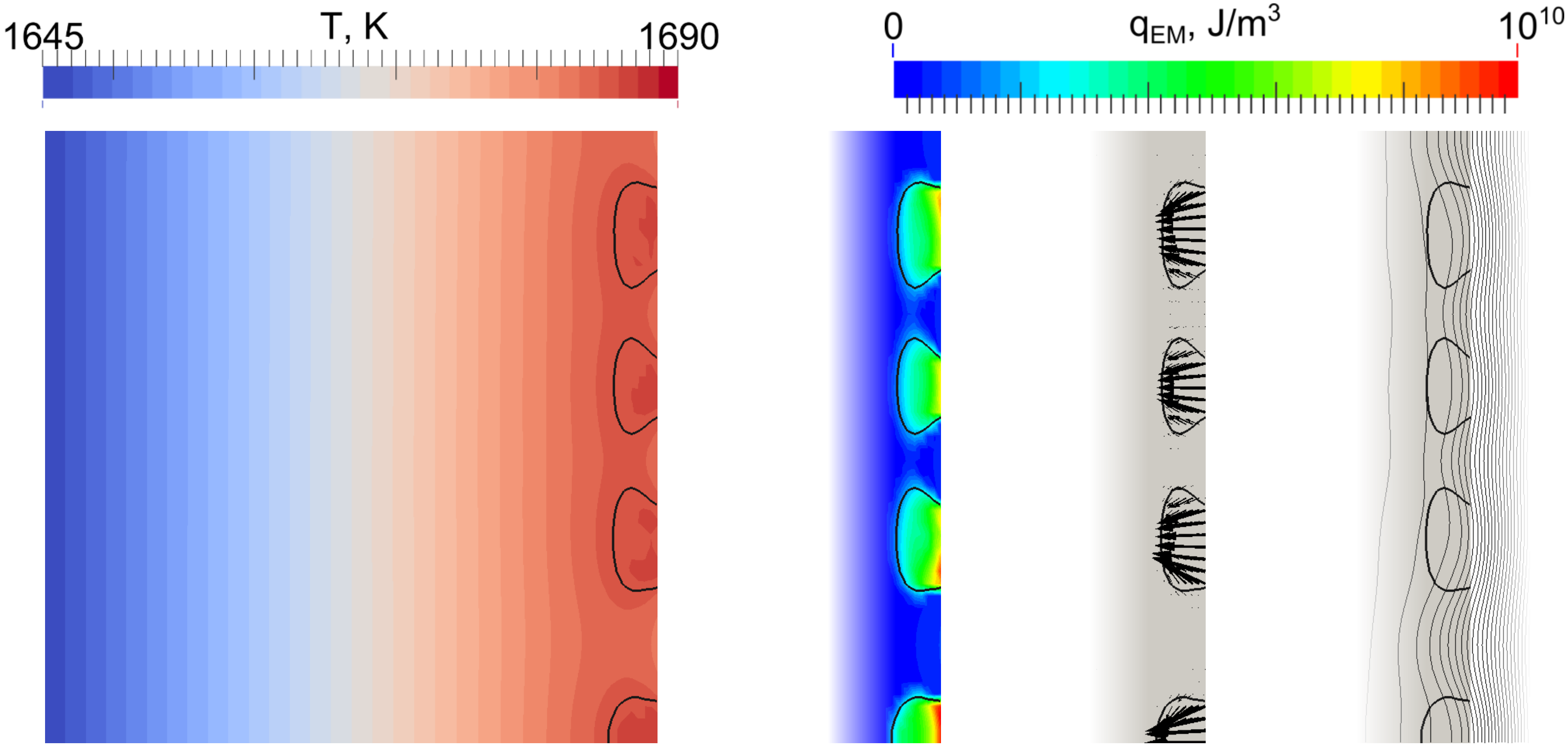

a) T **b)** q_{EM} **c)** $\vec{f}$ **d)** $|\vec{A}|$

Fig. 15: Temperature field, induced heat sources, Lorentz force density distribution and magnetic field lines in case with developed melt structures. Largest Lorentz force vector has modulus of $9 \cdot 10^5\ \mathrm{N/m^3}$.

Analysis of melt structure interaction with EM field

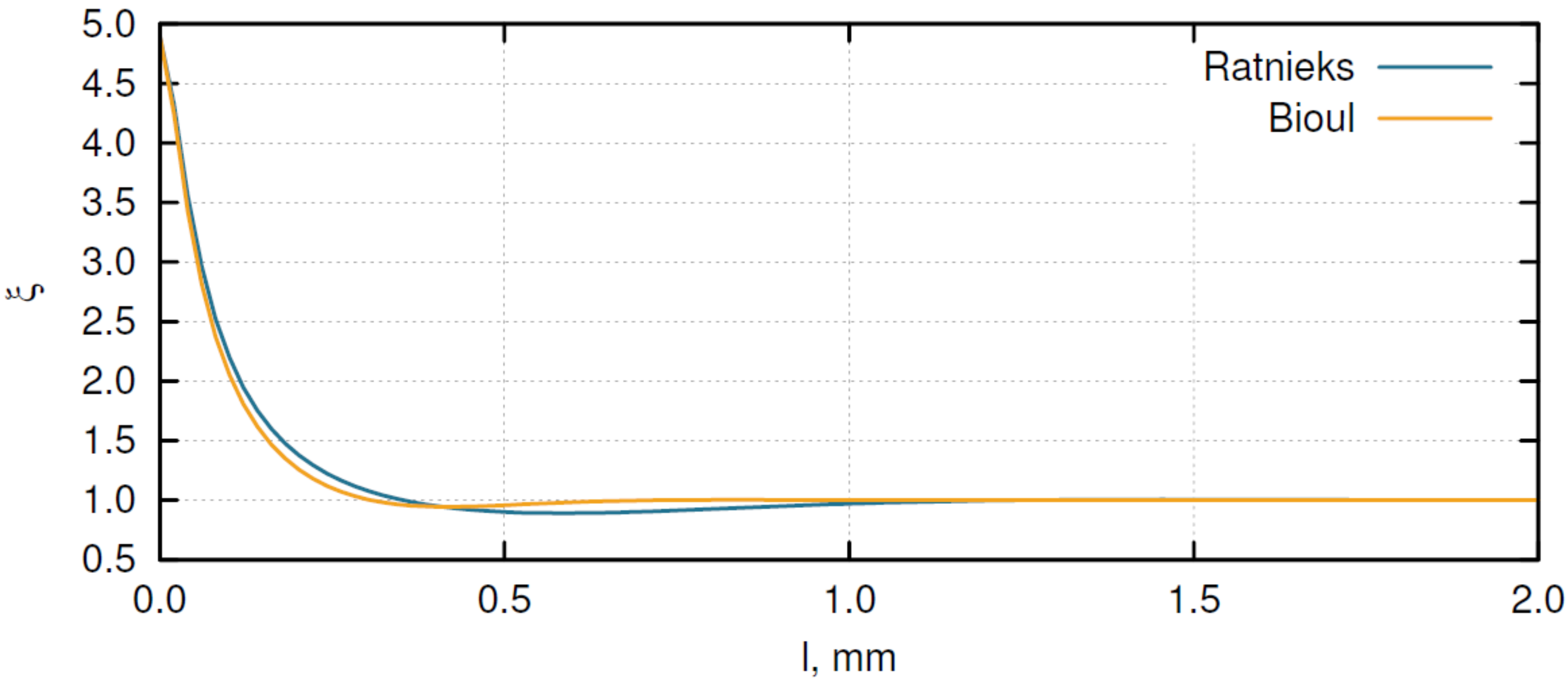

Fig. 16: Relative amount of induced heat sources ξ as function of melt layer thickness on top of solid silicon. Comparison between different analytical solutions[6,7] is given.

6 – **G. Ratnieks**. *Modelling of the Floating Zone Growth of Silicon Single Crystals with Diameter up to 8 Inch*. PhD thesis, University of Latvia, 2007.

7 – **F. Bioul**. *Use of Mathematical Expansions to Model Crystal Growth from the Melt under the Effect of Magnetic Fields*. PhD thesis, Université catholique de Louvain, 2007.

Analysis of melt structure interaction with EM field

$$Q_{\mathrm{EM}} = \iint\limits_{x,y=0\,\mathrm{mm}}^{x,y=5\,\mathrm{mm}} q_{\mathrm{EM}}\,\mathrm{d}x\,\mathrm{d}y$$

Volume of melt is about the same, but total induced heat is significantly different.

Type of phase distribution	Q_{EM}, kJ/m	ξ	ξ_{th}
uniform solid	14.80	5.07	4.90
homogeneous melt layer (0.25 mm)	3.39	1.16	0.90
melt structures (volume as 0.23 mm melt layer)	4.74	1.63	—
uniform melt	2.92	1.00	1.00

Fig. 17: Data of total induced heat Q_{EM} within the modelled silicon domain in case of different phase distributions. Same inductor current is used. Relative amount of induced heat ξ is also calculated (ratio with "uniform melt" case). Comparison to theoretical[6] value ξ_{th} is also given.

6 – **G. Ratnieks**. *Modelling of the Floating Zone Growth of Silicon Single Crystals with Diameter up to 8 Inch*. PhD thesis, University of Latvia, 2007.

Analysis of melt structure interaction with EM field

Fig. 18: Lorentz forces and magnetic field lines for calculation that was used to obtain melt free surface shape.

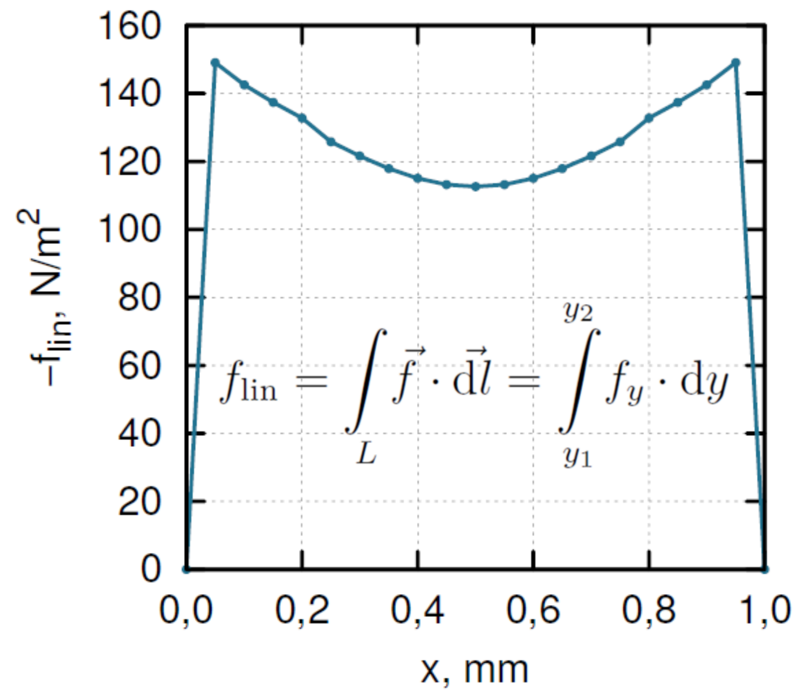

Fig. 19: Linear Lorentz force density along the melt surface (see Fig. 11).

Lorentz force influence on melt free surface shape

$$f_{\text{lin}} = k \cdot \gamma \qquad k = \frac{\left|\frac{\mathrm{d}^2 y}{\mathrm{d}x^2}\right|}{\sqrt{\left(1 + \left(\frac{\mathrm{d}y}{\mathrm{d}x}\right)^2\right)^3}}$$

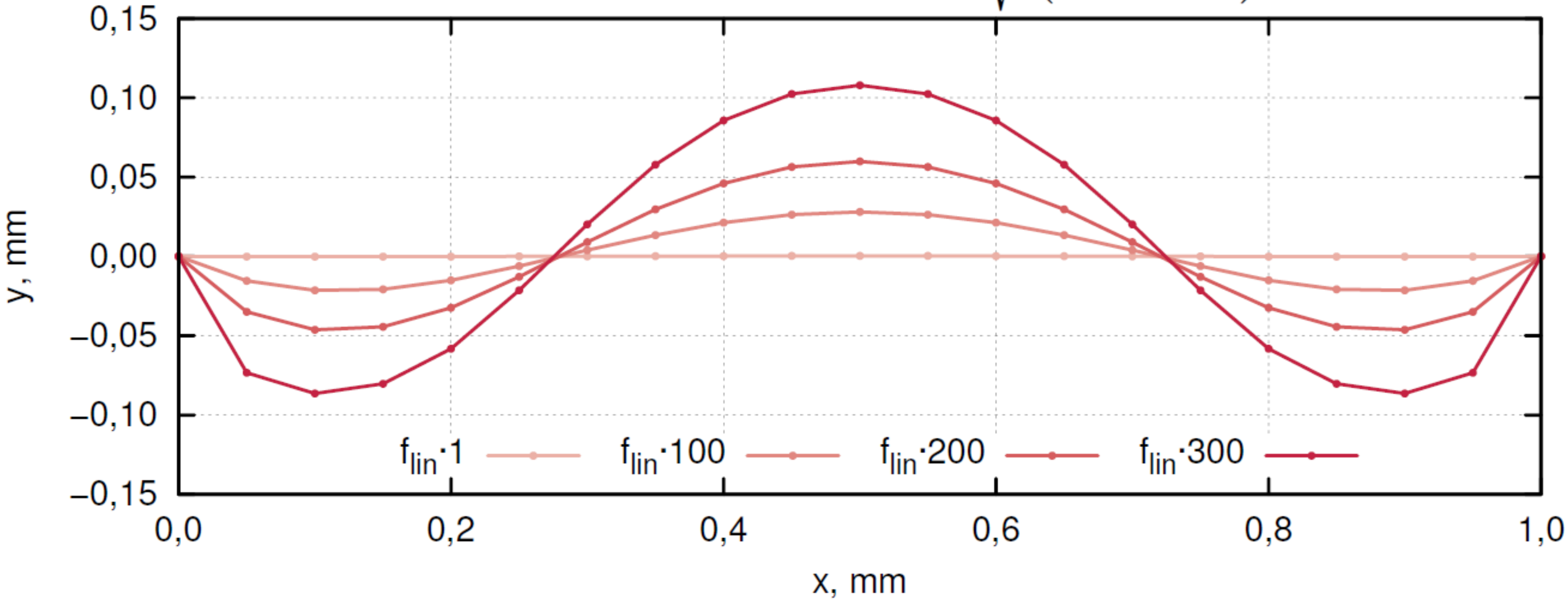

Fig. 20: Melt free surface shape calculated according to linear Lorentz force density balance with capillary forces. Several coefficients of magnitude were used to simulate different inductor currents.

Conclusions

- Melt pattern formation during inductive melting of Si is determined by the EM field interaction with two-phase environment with different electrical conductivities.
- Distance between melt structures is related to magnetic skin-depth in solid silicon.
- Presence of melt structures ensure greater total induced heat than homogenous layer with the same melt volume.
- Lorentz force influence on melt free surface shape is insignificant.

Further studies

- Melt free surface shape calculation by considering wetting angle $(30°)$ between silicon melt and solid.

- Melt removal from modelled domain and quasi-stationary melting process calculation.

- Creation of 3D model for the considered problem. Additional concentration of induced currents at the tips of melt regions could be obtained.

Transient calculation results with uniform initial temperature field

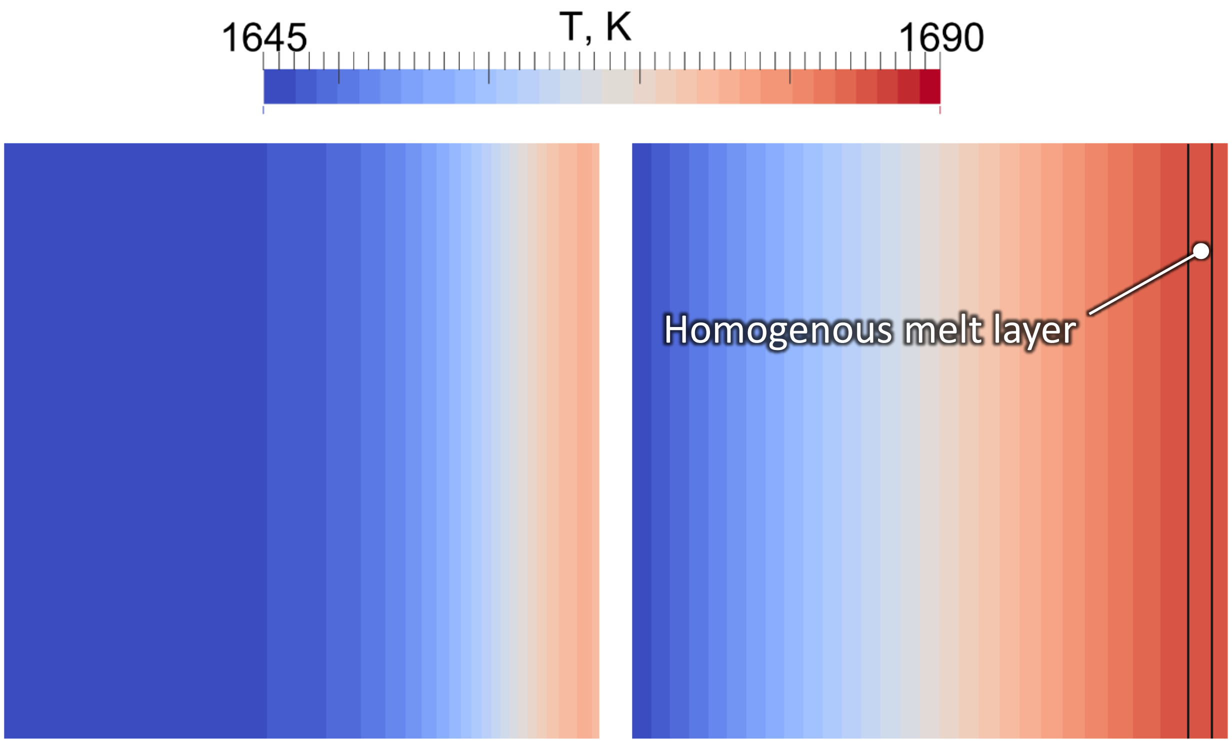

a) 30 ms **b)** 1000 ms

Fig. 21: Different time instances of calculated temperature fields. Black line represents phase boundary between silicon melt and solid.

Transient calculation results with non-uniform magnetic field

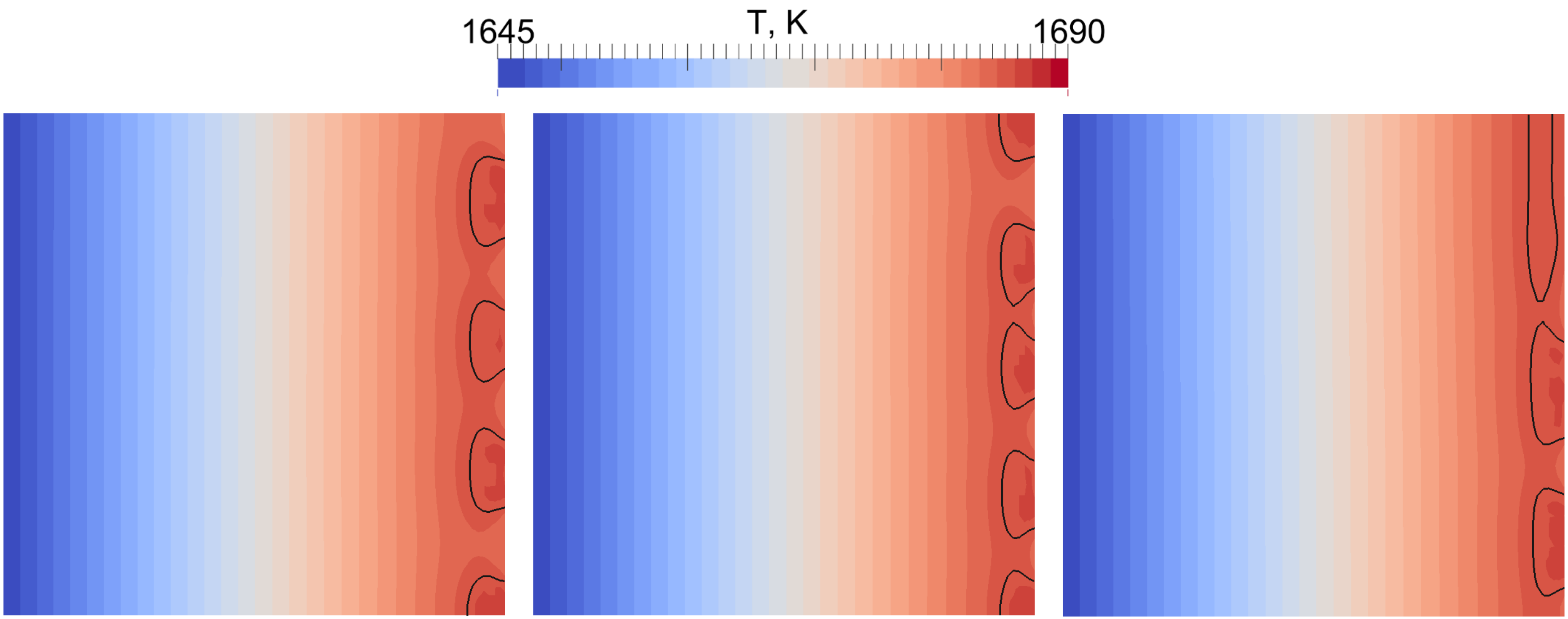

a) $A(x)$ from 0.99 to 1.01 **b)** $A(x)$ from 0.98 to 1.02 **c)** $A(x)$ from 0.95 to 1.05

Fig. 22: Calculation results obtained by using linear distribution $A(x)$ as magnetic vector potential boundary condition on the inductor surface.